In Vivo Biodistribution and Toxicology of Carboxylated Graphene Quantum Dots

Md Nurunnabi,[†] Zehedina Khatun,[‡] Kang Moo Huh,[§] Sung Young Park,[∥] Dong Yun Lee,[⊥] Kwang Jae Cho,[#,*] and Yong-kyu Lee[†,∥,*]

[†]Department of Polymer Science and Engineering, [‡]Department of Green Bioengineering, and [∥]Department of Chemical and Biological Engineering, Korea National University of Transportation, Chungbuk, 380-702, Republic of Korea, [§]Department of Polymer Science and Engineering, Chungnam National University, Daejeon 305-764, Republic of Korea, [⊥]Department of Bioengineering, Hanyang University, 222 Wangsimni-ro, Seongdong-gu, Seoul, 133-791, Republic of Korea, and [#]Department of Otolaryngology, Head & Neck Surgery, The Catholic University of Korea, College of Medicine Uijeongbu St. Mary's Hospital, Kyunggi-Do 480-717, Republic of Korea

ABSTRACT Photoluminescent graphene quantum dots (GQDs) have fascinating optical and electronic properties with numerous promising applications in biomedical engineering. In this work, we first studied the *in vivo* biodistribution and the potential toxicity of carboxylated photoluminescent GQDs. KB, MDA-MB231, A549 cancer cells, and MDCK normal cell line were chosen as *in vitro* cell culture models to examine the possible adverse effects of the carboxylated photoluminescent GQDs. The carboxylated GQDs are desirable for increased aqueous solubility. All cancer cells efficiently took up the carboxylated GQDs. No acute toxicity or morphological changes were noted in either system at the tested exposure levels. A long-term *in vivo* study revealed that the GQDs mainly accumulated in liver, spleen, lung, kidney, and tumor sites after intravenous injection. To reveal any potential toxic effect of the GQDs on treated mice, serum biochemical analysis and histological evaluation were performed. The toxicity results from serum biochemistry and complete blood count study revealed that the GQDs do not cause appreciable toxicity to the treated animals. Finally, we observed no obvious organ damage or lesions for the GQDs treated mice after 21 days of administration at 5 mg/kg or 10 mg/kg dosages. With adequate studies of toxicity, both *in vitro* and *in vivo*, photoluminescent GQDs may be considered for biological application.

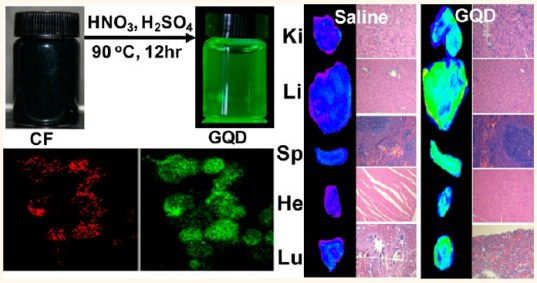

KEYWORDS: graphene quantum dots · biodistribution · toxicity · imaging · serum biochemistry

Graphene quantum dots (GQDs), as a new type of quantum dot, has attracted increasing attention due to their chemical stability, electronic properties, and photoluminescence.[1−6] Moreover, converting the 2-dimensional graphene sheets into 0-dimensional GQDs can enlarge the electronic and optoelectronic application because of the strong quantum confinement and edge effects.[7,8] Most works on GQDs have been focused on biomedical research, and experimental synthesis is only a recent effort.[9] Regarding the use of GQDs in biomedicine, there have been numerous reports of the development of graphene based biosensors aimed at detecting biomolecules with high sensitivities.[10] Owing to their ultrahigh specific surface area, GQDs with appropriate surface functionalization can be used for drug and gene delivery.[11−13]

Theranostic is defined as a material that combines the modalities of diagnostic imaging and therapy. It delivers therapeutic drugs and diagnostic imaging agents in one dose simultaneously. Theranostic strategies have the potential to overcome undesirable differences in biodistribution and selectivity that currently exist between distinct imaging and therapeutic agents.[14] Recently, a few groups have reported on graphene as a carrier for a drug delivery system, for example, hybrid SiO_2-coated quantum dots (HQDs)-conjugated graphene, for targeted cancer fluorescent imaging, tracking, and monitoring drug delivery, as well as cancer therapy.[15] The most promising aspect of utilizing GQDs as a theranostic nanoparticle are that they have high surface area-to-volume ratios, yielding high loading capacities. The wide planar surface of GQDs is considered an additional window for drug delivery as a number of drugs molecules could be located on both surfaces (top and bottom). The edge also could be conjugated with drug molecules through chemical

* Address correspondence to leeyk@ut.ac.kr.

Received for review April 24, 2013 and accepted July 2, 2013.

Published online July 05, 2013
10.1021/nn402043c

conjugation as reported earlier.[16] Additionally, nondegradable nanoparticles include them from being readily cleared through the kidneys without causing toxic moieties, depending on their surface functionalization. Thus, it is one of the most attractive materials to propel the biomedical field toward personalized medicine and imaging.

Recently, the potential toxicity of GQDs in biological systems has become a great concern, because nanotechnology related with graphene has shown great potential in disease diagnosis and imaging.[17] It has been reported in a number of previous studies that graphene or graphene oxide, without further surface modification, would cause severe pulmonary inflammation upon inhalation.[18] Graphene oxide (GO) intravenously injected into mice would also accumulate in the lung, resulting in pulmonary edema and granuloma formation.[19,20] On the other hand, surface functionalized graphene or GO with improved water dispersion and stability in physiological environments appears to be much less toxic in both oral and intravenous administration.[21,22] Christensen *et al.* have demonstrated that laser ablation-produced GQDs, with surface inactivation by polyethylene glycol, were able to quench and produce reactive oxygen species (ROS) in cell-free conditions, the latter occurring upon irradiation with blue light.[23] For the application of GQDs in biomedical areas, the surface modification of GQDs should be considered.[24−27]

To the best of our knowledge no report on *in vivo* imaging by GQDs has been reported to date. Toxicity related studies or results regarding biological application of GQDs also have not been reported to date. The GQDs are assumed to be safer than cadmium-based QDs based on elemental composition.[28,29] A thorough quantitative and qualitative *in vivo* toxicology analysis of GQDs, distribution, and clearance are required since this information will (i) determine the targeting efficiency of GQDs for diagnostics, (ii) allow for a better understanding of GQDs' nonspecificity toward tissues, (iii) allow for an assessment of GQD distribution and clearance that serves as the basis in determining their toxicity, and (iv) describe the interaction of GQDs with biological systems through blood and serum analysis.

In this study, we designed a new carboxylated photoluminescent GQD using citric acid, improving the aqueous solubility. Both the *in vivo* and *in vitro* imaging potentiality of green GQDs has been observed in different cell lines and animals, respectively. Imaging based biodistribution of GQDs has been observed to measure the qualitative and quantitative pharmacokinetics in KB tumor bearing nude mice. The synthesized nanoscaled (~5 nm) GQDs are suspected not to retain in the animal body for a long time. The GQDs nanoparticles are excreted from the biological system through glomerular filtration of the urinary system called renal excretion.[22] The results of various biochemical parameters of blood and serum demonstrated that the GQDs do not interact with the biological factors as the range of eight different factors are within the normal range and similar with animals treated by saline. The synthesized GQDs did not express any mentionable toxicity, biological interaction, or inflammatory symptoms in liver, kidney, heart, or spleen observed by histological analysis. Both *in vitro* and *in vivo* toxicity results demonstrate biosafety of GQDs for biological application.

RESULTS AND DISCUSSION

Preparation of Biocompatible Green GQDs. To make photoluminescent GQDs, exfoliation of carbon fiber first occurred during ultrasonication in acidic media, as reported previously.[30−37] Synthesis process of GQDs from carbon fiber is described in our previous report.[16] However, in brief, due to sonication in acid, the carbon fiber partially exfoliated and formed multilayered and/or monolayered graphene. The remaining multilayered graphene re-exfoliated during the reaction for 12 h at 95 ± 5 °C. These conditions facilitated the formation of a zigzag shaped graphene, showing an almost transparent gray-black color in solution. The hexagonal nanosized graphene structured particles are formed due to long-term exposure to strong acid and vigorous stirring as shown in Figure 1. A weak organic acid, citric acid, was then added to the reaction flask and stirring was continued for additional 1 h, at the same temperature, to introduce carboxyl groups (citric acid) on the surface of the GQDs. Water was slowly added to the flask after completing the reaction period; the color of the reaction mixture changed to reddish from brown. Sodium hydroxide (NaOH) was then slowly added to the beaker until the pH reached about 1. Sodium carbonate (Na_2CO_3) was added to adjust the pH to 8. The flask was placed in a ice bath to regulate the temperature to 4 °C. The soluton was precipitated by slowly stirring at the same temperature for 2−4 h. The precipitation was removed by decantation, and the liquid portion containing the photoluminescent GQDs was freeze-dried for 48 h. The entire process was performed to protect the GQDs from photobleaching.

Figure 1A shows a brief presentation of green colored hexagonal GQDs synthesized from carbon fiber. The figure shows that carbon fiber is black in color, even when in UV light, whereas the final product shows an excellent photoluminescent image due to UV excitation (365 nm). Figure 1B shows the photoluminescent (PL) intensity of GQDs, indicating the concentration-dependent PL intensity of the carboxylated GQDs at an emission wavelength of 510 nm. Fluorescence stability in both the buffer solution and serum solution is attributed to the fact that the fluorescence intensity of the carboxylated GQDs slowly decreased with respect to time (Supporting Information, Figure S1a). The results demonstrated that sufficient fluorescence intensity of the carboxylated GQDs remains for 3 days, due to their low stability in aqueous solution. Polymeric coating techniques may provide a solution to the loss of fluorescence intensity of the GQDs, improving

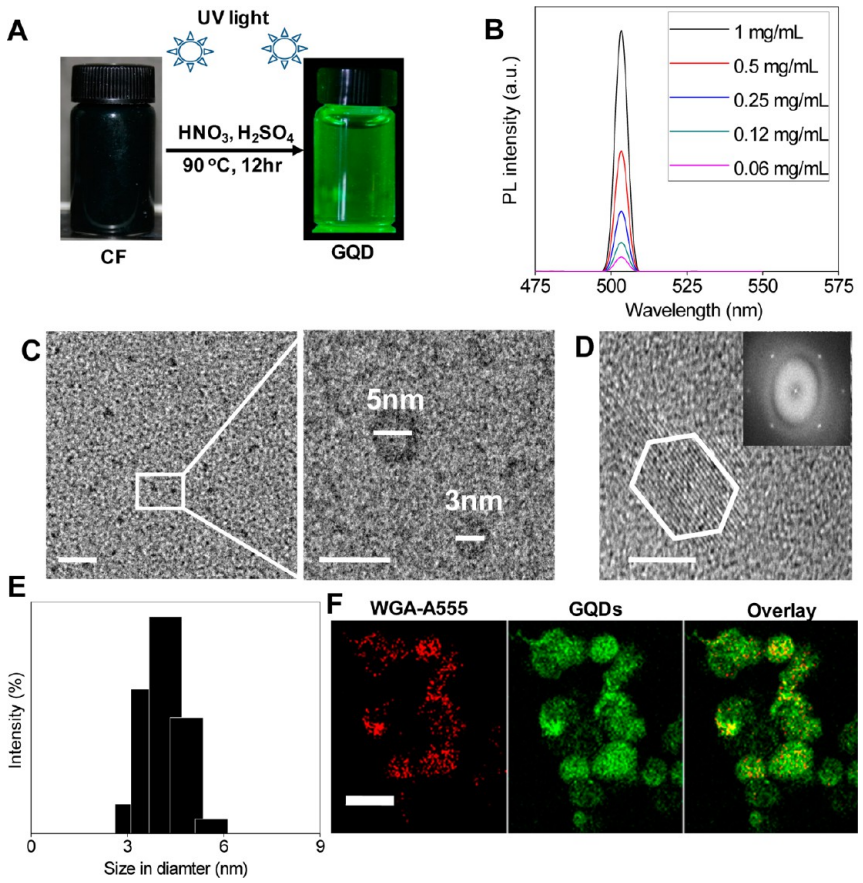

Figure 1. Characterization of the carboxylated GQDs. (A) Synthesis of PL GQDs from carbon fiber, (B) PL intensities of the carboxylated GQDs at 505 nm wavelength, (C) TEM images of the carboxylated GQDs shows the particle size being 3−5 nm (scale bar = 50 nm) and magnified images of GQDs (scale bar = 10 nm), (D) HR-TEM image showing the edge structure of lattices formed in GQDs and 2D fast Fourier transform pattern (inset image) (scale bar = 5 nm). (E) Size distribution of the carboxylated GQDs measured by DLS, and (F) confocal laser scanning microscopic (CLSM) images of KB cells treated with the carboxylated GQDs (scale bar = 50 μm).

their stability over the long-term. Figure 1C shows a HR-TEM image, showing that the synthesized GQDs are hexagonal in shape, with a lattice edge (inset picture). Size and morphology analysis indicated nanosized GQDs with a diameter of 3−6 nm, as measured by HR-TEM. The dynamic light scattering (DLS) data represent hydrodynamic sizes of the green GQDs as 3−6 nm in diameter (Figure 1D). From the size measurement of GQDs in FBS solution (10% FBS and 90% buffer solution), we found that the particle size simultaneously increased with time (see Supporting Information Figure S1b). To observe the cellular uptake of GQDs, the cell membranes of the KB cell were stained by wheat germ agglutinin (WGA) conjugated with AlexaFluor-555 (WGA-A555; Invitrogen). Confocal laser scanning images of KB (epidermal carcinoma) cancer cells demonstrate that the carboxylated GQDs can be taken through the cell membrane and retained inside the cell membrane as well as the cytoplasm (Figure 1E).

***In vitro* Cytotoxicity Test.** When the cell membrane is damaged during *in vitro* studies, intracellular lactate dehydrogenase (LDH) molecules are released into culture medium. Therefore, the LDH levels produced in cell cultures reflect cell membrane integrity. The GQDs were incubated with three different cell lines, KB, MDA-MB231, and A549, to observe the LDH release profile. LDH release amount from KB cells was observed to be higher compared to that from MDA-MB231, A549, and MDCK (madin−darby canine kidney epithelial cells) cells (Figure 2). The surface charge of nanoparticles and cell membranes plays an especially important role in cell−nanoparticle interactions. Several studies have demonstrated that the surface of MDA-MB231 and A549 cells are highly negatively charged, which is much higher than that of KB cells.[38−40] Another study shows that the higher is the negative charge of a particle, the higher is the cellular uptake to KB cell.[41] In this study we have observed that the zeta potential value of GQDs is −23.13 mV (presented in Supporting Information, Figure S2). Therefore, KB cells avidly incorporated those GQDs into subcellular vesicles, whereas MDA-MB231 and A549 cells did not efficiently take the GQDs. The release of LDH is directly proportional to the concentration of GQDs cocultured with the cell lines. An *in vitro* cytotoxicity study was carried out for different cancer cell lines KB, MDA−MB231, A549, and MDCK cells at different concentrations of GQDs (50, 100, 250, and 500 μg/mL) for 24 h as shown in Figure 2. The carboxylated GQDs were dispersed in phosphate buffer saline (PBS) and were

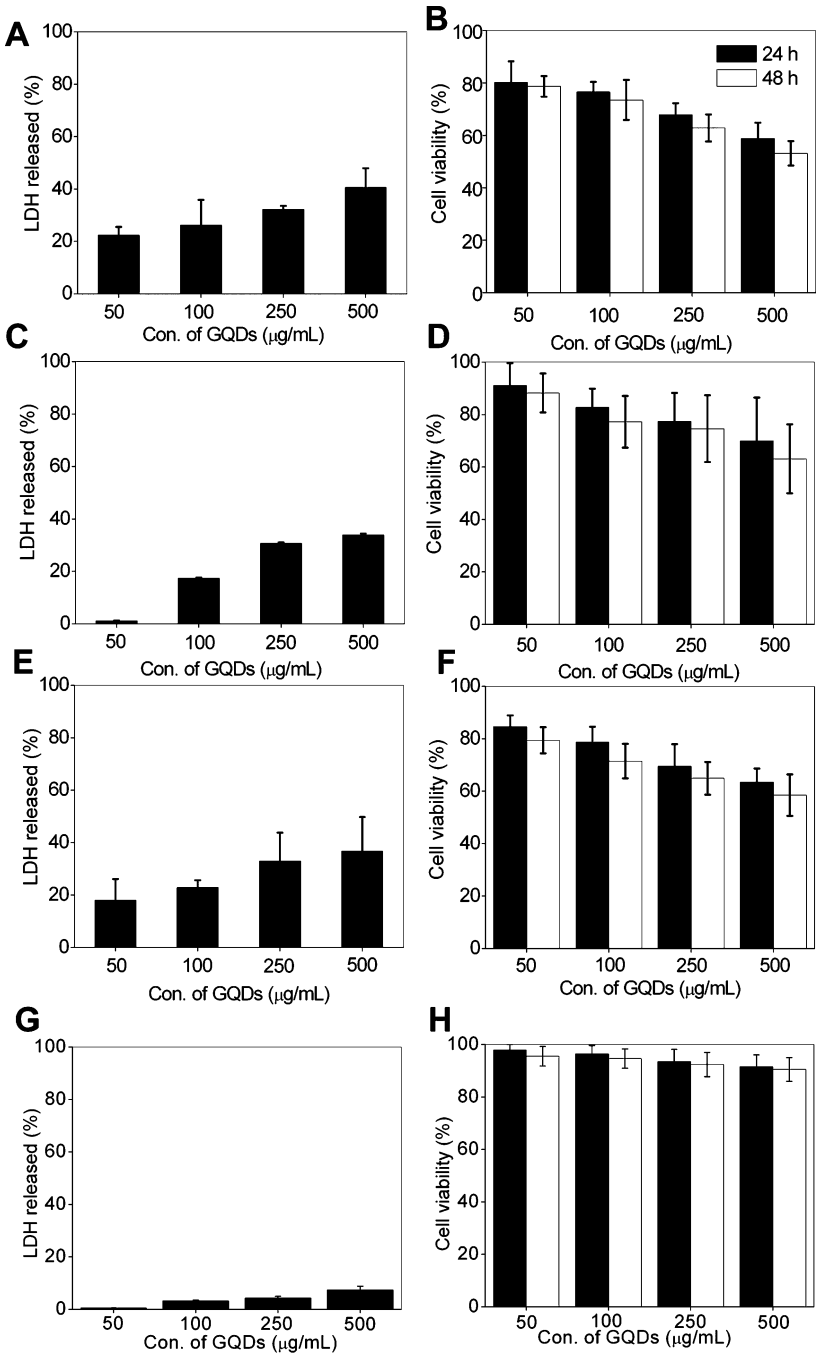

Figure 2. *In vitro* **cytotoxicity test. Lactate dehydrogenase (LDH) release study and MTT assay of KB (A and B), MDA-MB231 (C and D), A549 cancer cells (E and F), and MDCK normal cells (G and H) treated with the carboxylated GQDs, respectively. The graphs show the cell viability of the GQD-treated MDCK cell is more than 90%. LDH release of the GQD-treated MDCK cell is relatively lower than those of the cancer cells. Data represent mean ± SEM (n = 6) (p < 0.05, one-way ANOVA).**

cocultured with the cell lines, after which the cell viability was measured by MTT colorimetric assay. The results of the cell viability test demonstrate that the GQDs did not exert any mentionable toxicity as the cell viability was more than 80% even at a relatively high concentration (500 μg/mL) of GQDs (Figure 2). However, the cell viability of KB cells was less than that of MDA-MB231 and A549 cells under the same conditions (concentration, duration, and incubation time). Both MTT assay and LDH release test demonstrated that human epidermal cancer cells are more sensitive to GQDs compared to breast cancer cells (MDA-MB231) and human epithelial cancer cells (A549). After treating MDCK cells with the GQDs, it was revealed that the nonspecific GQD nanoparticles do not show any potential toxicity, showing low LDH release amount (below 4%) and high cell viability (above 95%). The result also demonstrates that the carboxylated GQDs may not be taken by the normal cells and therefore do not cause appreciable toxicity. One of the remaining issues with cadmium-based quantum dot probes is their potential

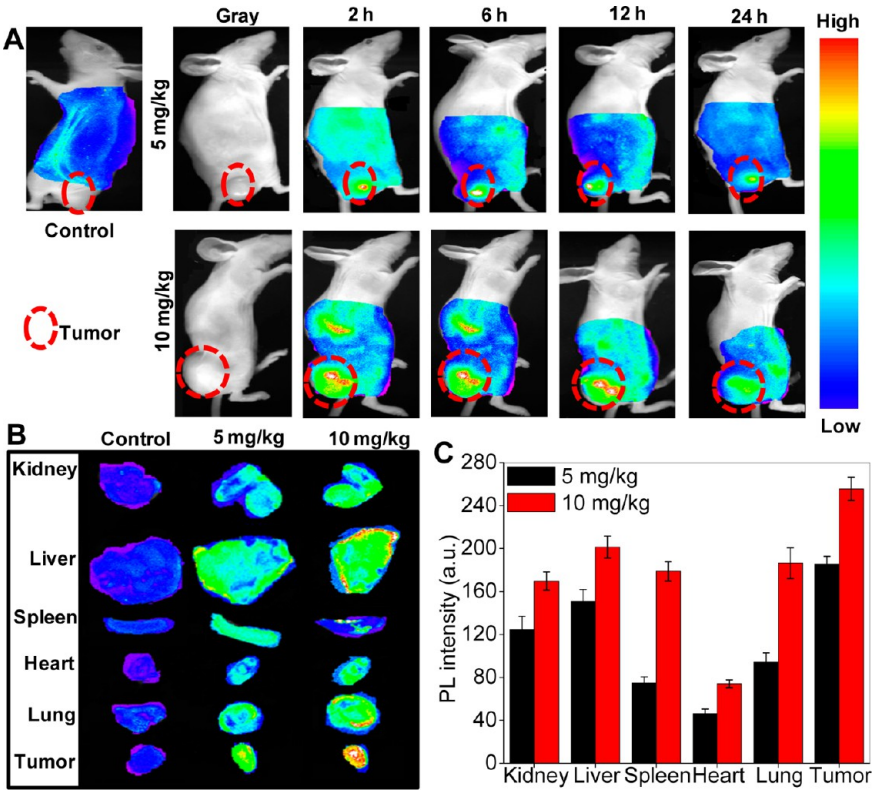

Figure 3. ***In vivo*** **imaging and biodistribution of the carboxylated GQDs. (A) The** ***in vivo*** **imaging of KB tumor bearing mice after intravenous injection of GQDs (5 and 10 mg/kg), (B)** ***ex vivo*** **images of isolated organs of mice at 24 h after injection of each carboxylated GQDs, and (C) PL intensities of the carboxylated GQDs from isolated organs at different dosages (5 and 10 mg/kg). The data represent mean ± SEM (*n* = 3) (*p* < 0.05, one-way ANOVA).**

in vitro and *in vivo* toxicity. For example, CdSe nanocrystals are highly toxic to cultured cells under UV illumination, showing release of Cd ion. However, the GQD has relatively low toxicity and high cell viability as measured by MTT assay.

In vivo **and** ***ex-vivo*** **optical imaging and biodistribution study.** To further evaluate the optical imaging and biodistribution of GQDs in mice, the carboxylated GQDs were injected into tumor bearing Balb/c nude mice. The tumor implantation method has been described elsewhere.[42] The noninvasive imaging of GQDs in mice was performed using a Kodak Molecular Imaging System (KLMS) (4000MN PRO, Kodak, USA).[43] Figure 3A shows time-dependent *in vivo* optical images of the mice after the injection of green GQDs (5 and 10 mg/kg dosage). Immediately following the intravenous injection of the carboxylated GQDs, no signals were captured from the deep tissues or organs such as heart, liver, or spleen at 505 nm in emission wavelength. However, at 12 h postinjection a fluorescence signal was observed at the tumor site, as captured by the molecular imaging systems. The results demonstrated that the green GQDs could be used for superficial tissue imaging, such as skin cancer detection. The nanosized GQDs were accumulated by the tumor through the reticule endothelial system (RES) as the GQDs are not target specific. As blood circulated, the fluorescence decreased gradually. At 24 h of postinjection no fluorescence signal was observed from the tumor, or from any other portion of the body. The probable reason for this profile is either rapid excretion from the body due to the nanosize of the carboxylated GQDs (3−6 nm in diameter), or due to a loss of fluorescence intensity with time. The results may demonstrate that the free GQDs excrete from the animal body through kidney as the particle sizes of the GQDs were around ∼5 nm in diameter.[44] An analysis of the dissected organs of nude mice injected with the carboxylated GQDs, revealed accumulation of the GQDs, primarily in the liver, and also in the heart, at 2 h of postinjection. The liver accumulation was observed to decrease steadily over time, and the kidney accumulation greatly increased 12 h postinjection as observed from the *in vivo* and *ex vivo* images of the carboxylated GQD-treated mice. The *ex vivo* images of isolated organs were also observed by the optical imaging system, to evaluate the biodistribution of intravenously injected GQDs. The results attribute that the GQD nanoparticles were distributed over the entire body through systemic circulation and were concentrated in different organs up to 12 h postinjection. PL intensity at 24 h postinjection was lower than that at 12 h postinjection, which is likely due to the excretion of GQDs (Figure 3B). Figure 3C demonstrates the quantitative analysis of biodistribution, showing GQD accumulation in liver, lung, and spleen at 2 h postinjection.

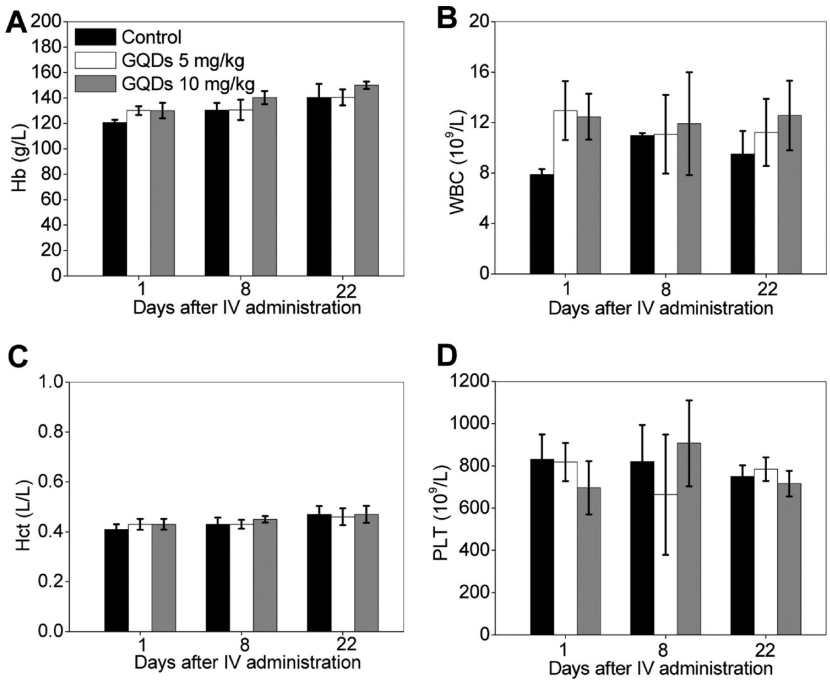

Figure 4. Complete blood count test in rats. A–D results indicate mean ± SEM (n = 6) of (A) Hb, (B) WBC, (C) Hct, and (D) PLT. The results demonstrate that the values of Hb and Hct are the same with the control, keeping within the normal ranges. The values of WBC and PLT are partially fluctuated compared to the control but remain within the normal ranges. Control means the blood samples of rats treated with saline (n = 6) (p < 0.05, one-way ANOVA).

Complete Blood Count and Serum Biochemistry Analysis. *In vivo* cytotoxicity studies of the carboxylated GQDs were performed on rat model for 22 days. The free GQDs were suspended in PBS and injected via the tail vein every 2 days for 22 days (total seven injections) at the same time saline was administered to the control rat. Blood was collected from the rat, and the serum was separated by centrifugation. Because the carboxylated GQDs are similar in size to viruses and small proteins, they may affect the immune system or induce an inflammatory response, which would be indicated by changes in hematological factors, such as red and white blood cell count, etc. Accordingly, standard hematological and biochemical markers were monitored. For the hematology study, we have selected the important markers of hemoglobin (Hb), white blood cells (WBC), hematocrit (HCT), and platelet count (PLT). A complete blood count (CBC) was performed at regular intervals, and the results did not suggest any acute toxicity (Figure 4A–D). Only a negligible variation was observed in WBC values. Though the value of WBCs was higher for animals treated with the carboxylated GQDs than that of control animals, the range was still within normal levels.

To monitor for any potential toxic effect of the carboxylated GQDs on the treated rats, we carried out a serum biochemistry study. Blood was collected from the GQDs and saline (control) treated rats at 1, 8, and 22 days of observation, whereas the the GQDs were administered to the rats after every 2 days. Then indicators of kidney function, blood urea nitrogen (BUN), and creatinine (CRE), were also normal (Figure 5A, B). Specifically, normal urea levels in blood indicate the general condition of the kidney and liver, and damage or disorder to renal function may be identified by higher or than the normal levels of urea in the blood and liver diseases or damage or malnutrition of liver indentified by lower than normal level.[45] As shown in Figure 5 panels A and B, both BUN and CRE values are within normal ranges, and are similar to those of control animals. The seven important hepatic indicators—albumin (ALB), globulin (GLOB), glutamic pyruvate transaminase (GTP),alkaline phosphatase (ALP), glutamic oxaloacetic transaminase (GOT), total bilirubin (TB), and total protein (TP) were measured periodically, and showed no sign of liver injury (Figure 5C–I). The hepatic factors indicated normal liver function, as the values of parameters were within normal ranges and were similar to values of control animals (treated with saline solution).

Histological Analysis of Animal Tissues. Histological analysis identifying the carboxylated GQD nanoparticles allows for a detailed microscopic evaluation and histological assessment of tissue interactions. The data provide visual observation of inflammation or lesions caused by IV administered GQD nanoparticles. From the histological analysis of animal tissues, there are no apparent histopathological abnormalities or lesions observed in the heart, kidney and spleen (Figure 6). The H&E staining images of such organs showed the same properties as those of control animals. Histological examination did not show any severe symptoms of toxicity but moderate pathological changes were observed in

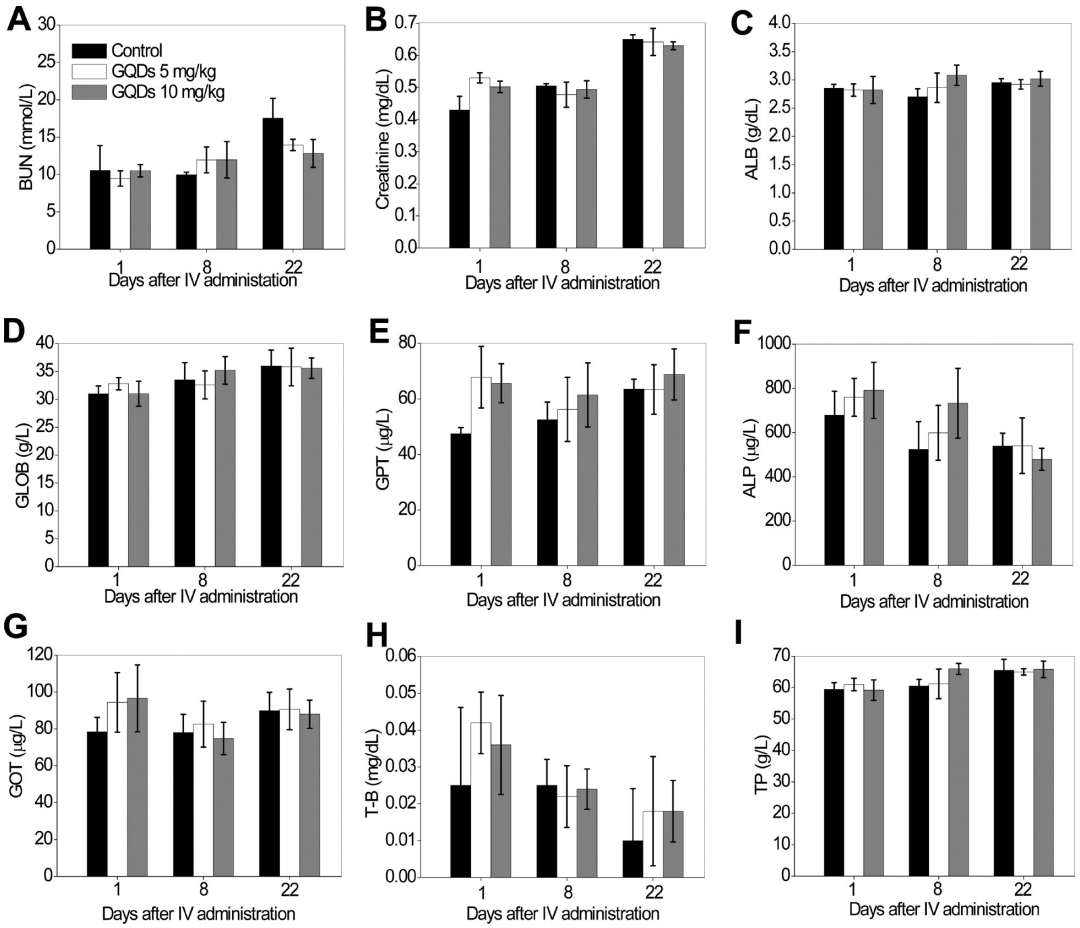

Figure 5. Serum biochemistry results from rats treated with the carboxylated GQDs. A−I results indicate mean ± SEM ($n = 6$) of (A) BUN, (B) CRE, (C) ALB, (D) GLOB, (E) GTP, (F) ALP, (G) GOT, (H) TB and (I) TP. Control means the serum samples of rats treated with saline ($p < 0.05$, one-way ANOVA).

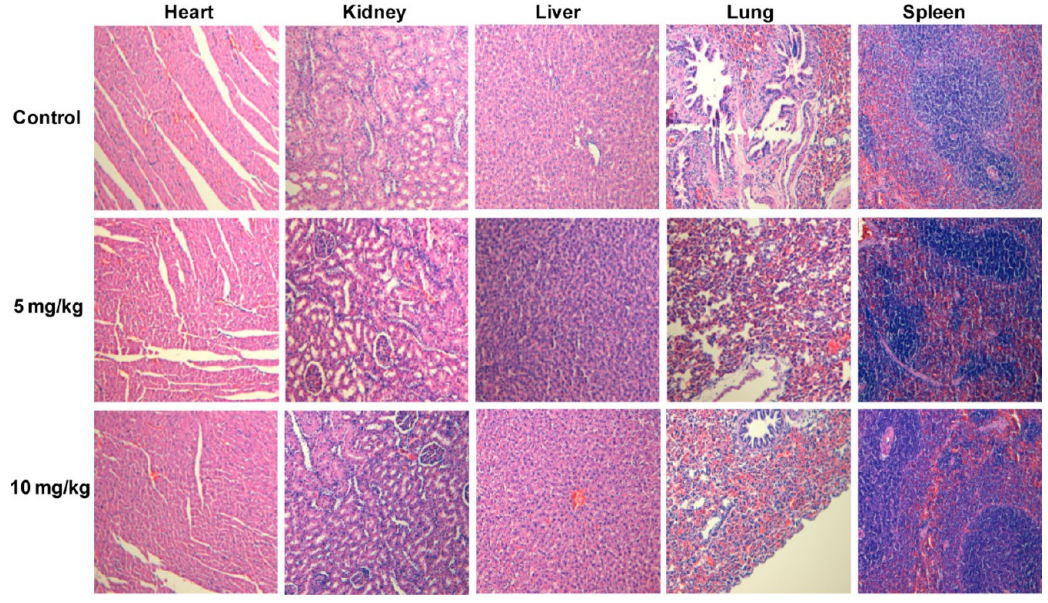

Figure 6. Histology study to measure toxicity. Histological evaluation of the major organs of the mice at 22 days after intravenous injection of the GQDs. No symptoms of inflammation and/or lesion were observed in the images. Tissues of 5 and 10 mg/kg GQDs treated mice are similar with that of tissues of saline treated mice. Images were taken at 160× magnification with hematoxylin and eosin staining.

the liver and lung at 21 days after the carboxylated GQD nanoparticle administration at a higher dose (10 mg/kg). Histological analysis at 1 and 8 days post injection revealed no pathological changes in the heart, lung, kidney, liver or spleen (Figure S3 and Figure S4). Hepatocytes in the liver samples were observed to be normal, and there were no signs of inflammatory response. No pulmonary fibrosis was detected in the lung samples. The glomerulus structure in the kidney section was observed without difficulty. Necrosis was not found in any of the histological samples which were analyzed. Body weights were monitored every other day, and the fluctuations were not greater compared to those of the control group. The result suggests no adverse effects of GQDs, as body weight of GQDs treated animal was similar as saline treated animal (Figure S5).

CONCLUSION

No acute toxicity or morphological changes were noted from *in vitro* cytotoxicity studies of the carboxylated GQDs as determined by both LDH and MTT assay. The *in vivo* and *ex vivo* optical imaging of nude mice and isolated organs demonstrated that the carboxylated GQDs accumulated in the liver, spleen, kidney, and tumor at 24 h after intravenous injection of GQDs. The carboxylated GQDs do not cause apparent toxicities in rats at different dosage (5 and 10 mg/kg) for 22 days as evidenced by blood biochemistry and hematological analysis. No severe symptoms of inflammation were observed in the liver, kidney, spleen, heart, or lung at 22 days after the administration of the carboxylated GQDs nanoparticles. Our findings are highly encouraging, providing substantial evidence of the safety of GQDs for biomedical application.

EXPERIMENTAL SECTION

Materials. Pitch carbon fiber was purchased from FiberGlast Development Corporation (Carr Drive Brookville, OH). Sulfuric acid, nitric acid, sodium hydroxide, and sodium carbonate was purchased from Sigma–Aldrich (St. Louis, MO). Cell culture reagents, including fetal bovine serum (FBS), Dulbecco's Modified Eagle Medium (DMEM), penicilline/streptomycin, trypsin/EDTA, and Dulbecco's phosphate buffer saline (PBS), were purchased from Gibco BRL (Carlsbad, CA, USA). 3-(4,5-Dimethylthiazol-2-yl)-2 and 5-diphenyl tetrazolium bromide (MTT) were obtained from Amresco, Inc. (Solon, OH, USA).

Synthesis and Characterization of Green Photoluminescent GQDs. The preparation of photoluminescent GQDs from carbon fiber was reported previously by Peng and his co-workers.[46] We have partially modified and optimized that process in this research. In brief, carbon fibers (100 g) were added to 40 mL of sulfuric acid, and the solution was sonicated for 1 h at room temperature. The solution was injected slowly to a mixture of nitric acid (20 mL) and sulfuric acid (450 mL) at 95 °C. The reaction was carried out for 12 h to make photoluminescent graphene. To introduce carboxyl groups on the surface of the graphene, citric acid (100 mg) was added, and stirring was continued for 1 h at 60 °C. After reaction, an excess amount of water (200 mL) was added to the solution. Sodium hydroxide and sodium carbonate were then added to the solution to bring it to pH 8. The solution was placed in an ice bath and the temperature was controlled to ~4 °C with slow stirring. Precipitation was separated from the solution by decantation. The final product was freeze-dried for 3 days to obtain a fine powder. The size distribution and morphologies of GQDs nanoparticles were examined using dynamic light scattering (DLS) (ELS-Z2, Otsuka Electronics Co., Ltd., Japan) and a TEM (JEOL, Japan), respectively. Photoluminescence, excitation, and emission were measured using a luminescent analyzer Fluoro Mate FS-2 (Scinco, Korea) The XRD data were collected on a Rigaku D/Max Ultima II Powder X-ray diffractometer (Rigaku Corporation, Japan).

***In Vitro* Stability of GQDs.** To investigate the stability of the carboxylated GQD nanoparticles, we measured changes in the fluorescent intensity and average size of GQDs nanoparticles in serum, at different pH values (5, 7, and 9) in 0.1 M PBS buffer, respectively. The carboxylated GQD nanoparticles were separately dispersed into each pH buffer solution (1 mg/mL) for 2 h. The average diameter of the GQDs nanoparticles was then measured using a DLS (ELS-Z, Otsuka Electronics Co., Ltd., Tokyo). To minimize interference by large molecules in FBS, the serum solution was filtered using a 0.45 μm filter membrane. The GQDs nanoparticles were then incubated in the FBS solution for 5 days, and any change in size was monitored.

***In Vitro* Cytotoxicity Evaluation and Cell Imaging.** An *in vitro* cytotoxicity study of the carboxylated GQD nanoparticles was carried out using KB, MDA-MB231, A549, and MDCK cells for 24 and 48 h, respectively. At 37 °C and 5% CO_2 in a humidified atmosphere, cells were grown in a medium containing MEM with 10% fetal calf serum. The cells (5×10^4 cells/mL) were grown in a cell culture flask and were harvested by 0.25% trypsin–0.03% EDTA solution. An sample of 200 μL of cells was placed in 96 well plates and incubated for 24 h. After 24 h, the complete medium was suctioned, and the carboxylated GQDs were added to the wells at different concentrations (50, 100, 250, and 500 μg/mL) with complete medium. For the cell viability assay, MTT solution aliquots at 5 mg/mL in PBS were prepared, followed by culture incubation with this solution at 5% in the culture medium for 4 h in an incubator, with a moist atmosphere of 5% CO_2 and 95% air at 37 °C. After 4 h, 100 μL of MTT solubilizing solution was added, and the solution was gently shaken for 15 min. Finally, the absorbance of MTT colorimetric assay was measured by Varioskan flash (Thermo Scientific, USA) at a wavelength of 570 nm. The viable quantity of cells was calculated by the following equation:

$$\text{cell viability (\%)} = \frac{\text{absorbance of sample cells}}{\text{absorbance of control cells}} \times 100$$

To observe the cellular uptake and transfection properties of nanosized GQDs, they were dispersed in PBS (100 μg/mL) and cocultured with KB cells, incubated for 1 h, and washed with saline to remove any unbound particles. Cells were fixed for 5 min at room temperature using DPBS containing 4% (v/v) paraformaldehyde and 0.3% (v/v) glutaraldehyde. Cell membranes were stained using 1 μg/mL wheat germ agglutinin (WGA) conjugated with AlexaFluor-555 (WGA-A555; Invitrogen) in 5% (w/v) goat serum (GS) for 45 min at room temperature in the dark followed by subsequent washing with DPBS (Invitrogen). The cells were reincubated for 30 min at room temperature in the dark followed by washing with DPBS. The fluorescence images were taken by confocal laser scanning microscope (CLSM) with multilaser and excitation conditions. The images were taken at ×40 magnification, using a 555/514 nm (WGA-A555/GQDs) excitation filter to get images of both membrane and GQDs uptake by KB cells.

Lactate Dehydrogenase (LDH) Release Assay. The LDH test-kit (CytoTox 96 Non-Radioactive Cytotoxicity Assay, Promega Co.) was used to assess the cell membrane integrity. KB, MDA-MB231, A549, and MDCK cells were plated in the 96-well plates (5×10^3 cells/well) and were incubated for 24 h. The GQD samples were introduced separately to the cells at different concentrations (50, 100, 250, and 500 μg/mL), and the test

cultures were incubated for another 24 h. The positive control was prepared by adding 10 μL of cell lysis solution (Cell Signaling Technology, MA, USA) to the control cells 45 min prior to centrifugation. Cultures were then centrifuged (1200 rpm $\times$ 5 min), after which 100 μL of supernatant was taken out from each well for LDH assay, following the instruction of the kit. The absorbance at 490 nm was recorded on a Microplate Reader (Thermo, Varioskan Flash, MA, USA). The LDH leakage (% of positive control) is expressed as the percentage of (test $-$ blank)/(positive $-$ blank), where test is the cells exposed to the carboxylated GQDs, positive is the optical density of the positive control cells, and blank is the optical density of the wells without cells.

Noninvasive Optical Imaging Study. Six to seven week-old SKH1 female nude mice (weight range of 21$-$25 g) were purchased from Orient Bio Inc., (Seoul, Korea) and were maintained under specific pathogen-free conditions. All experiments were approved by the institutional guidelines of the Institutional Animal Care and Use Committee (IACUC) of the Catholic University of Korea College of Medicine, in accordance with NIH guidelines. Human breast cancer KB cell lines (Korean Cell Line Bank, Korea) were trypsinized, washed twice with serum free RPMI 1640, and suspended at a density of 5×10^7 cells/mL PBS.[47] An amount of 100 mL of the suspended cells was subcutaneously injected into the back of the mice. On day 21 after tumor injection, the resulting tumors reached a volume of 140$-$160 mm^3. For *in vivo* imaging studies, tumor-bearing mice were administered 2.5 and 5 mg/kg of the carboxylated GQD nanoparticles intravenously (IV). Mice were anesthetized with ketamine (87 mg/kg, Virbac Laboratories, France) and xylazine (13 mg/kg, Kepro B.V., Netherland) via intraperitoneal injection. Noninvasive images of the carboxylated GQD injected mice were taken by a time-domain diffuse optical tomography system. Mice were placed on the imaging platform, and images were taken at 2, 4, 6, 8, 10, 12, and 24 h postinjection. The 3D scanning region of interest was selected using a bottom-view charge-coupled device (CCD).[48,49] All images were taken using the Kodak *in vivo* imaging system (4000MN PRO, Kodak, USA).

Complete Blood Count (CBC) and Clinical Biochemistry Panel Analysis. The animals were randomly divided by three different experimental groups (control, 5 mg/kg, and 10 mg/kg of the carboxylated GQDs), each group containing six rats. To observe the CBC and serum biochemistry, GQD nanoparticles (5 and 10 mg/kg) were intravenously administered to the SD rat (220$-$225 g body weight) for 22 days with a two days interval between each injection (7 dosages for 22 days). The rats were purchased from Orient Bio Inc., (Seoul, Korea) and were maintained under specific pathogen-free conditions. All experiments were approved by the institutional guidelines of the Institutional Animal Care and Use Committee (IACUC) of the Catholic University of Korea College of Medicine, in accordance with NIH guidelines. Blood samples were collected at 1, 8, and 22 days of observation, while the saline and/or GQD nanoparticles were administered after every two days up to 22 days. On day 1, 8, and 22 the rats were sacrificed and a total of 5 mL of whole blood was collected from heart puncture; 2 mL of whole blood was collected in 10% EDTA for complete blood count, and the remaining 3 mL of blood serum was used for a biochemistry panel assay. Each blood sample (2 mL) was put in an anticoagulant (EDTA) coated bottle (K3EDTA bottle, ACUETTER, Greiner, Austria) to prevent coagulation. The blood sample was then analyzed for counting the number of white blood cells (WBC), hemoglobin, hematocrit, and the number of platelets by an automated hematology analyzer (Sysmex XE-2100, Japan). The other whole blood sample of 3 mL was put into a Z Serum Sep Clot Activator bottle (VACUETTER, Greiner, Austria) and was centrifuged at 3000 rpm for 7 min. Afterward the supernatant (serum) was taken for biochemistry analysis. We determined serologic parameters related to liver and kidney function, including the level of various enzymes, such as aspartate aminotransferase (AST), alanine aminotransferase (ALT), alkaline phosphatase (ALP), total protein, albumin, globulin, total bilirubin (TB), blood urea nitrogen (BUN), and creatinine (Cr). Total protein, albumin, and globulin were assayed by the Bradford method. For each sample, 200 μL serums were mixed in 800 μL of Bradford reagent. Optical density was then measured (at 600 nm) in the dark after 10 min incubation. Bovine serum albumin was used as a standard protein. Assay for AST, ALT, and ALP was performed using an enzyme assay kit, and data were obtained using a spectrophotometer (Hitachi 7600).

Histological Analysis. The harvested heart, liver, spleen, lung, and kidney of rats were fixed with 4% paraformaldehyde for 4 h after washing with saline, and were then dehydrated. Afterward organ samples were embedded in paraffin, sectioned (4 μm), and stained with hematoxylin and eosin (H&E). The stained slides were examined by light microscopy through a 160$\times$ objective lens. To determine the toxicity of the carboxylated GQD nanoparticles, a histological analysis of organs was performed to determine whether or not the GQD nanoparticles or the degradation of the carboxylated GQDs caused tissue damage and/or any pathologic impacts such as inflammation or necrosis.

Conflict of Interest: The authors declare no competing financial interest.

Acknowledgment. This research was supported by Basic Science Research Program through the National Research Foundation of Korea (NRF) funded by the Ministry of Education, Science and Technology (2010-0021427).

Supporting Information Available: Additional figures of stability profile of GQDs, histological analysis data and body weight of rat. This material is available free of charge *via* the Internet at http://pubs.acs.org.

REFERENCES AND NOTES

1. Luk, C. M.; Tang, L. B.; Zhang, W. F.; Yu, S. F.; Teng, K. S.; Lau, S. P. An Efficient and Stable Fluorescent Graphene Quantum Dot$-$Agar Composite as a Converting Material in White Light Emitting Diodes. *J. Mater. Chem.* **2012**, *22*, 22378–22381.
2. Yan, X.; Cui, X.; Li, L-s. Synthesis of Large, Stable Colloidal Graphene Quantum Dots with Tunable Size. *J. Am. Chem. Soc.* **2010**, *132*, 5944–5945.
3. Zhi-Dong, Y.; Wei, L.; Xian-Long, G. Electronic Properties on the Point Vacancy of Armchair Edged Graphene Quantum Dots. *Acta Phys. Sin.* **2012**, *61*, 117105–117110.
4. Shi, H.; Barnard, A. S.; Snook, I. K. Quantum Mechanical Properties of Graphene Nano-flakes and Quantum Dots. *Nanoscale* **2012**, *4*, 6761–6767.
5. Ritter, K. A.; Lyding, J. W. The Influence of Edge Structure on the Electronic Properties of Graphene Quantum Dots and Nanoribbons. *Nat. Mater.* **2009**, *8*, 235–242.
6. Sun, H.; Wu, L.; Gao, N.; Ren, J.; Qu, X. Improvement of Photoluminescence of Graphene Quantum Dots with a Biocompatible Photochemical Reduction Pathway and Its Bioimaging Application. *ACS Appl. Mater. Interfaces* **2013**, *5*, 1174–1179.
7. Lu, Q.; Huang, R. Nonlinear Mechanics of Single-Atomic-Layer Graphene Sheets. *Int. J. Appl. Mech.* **2009**, *3*, 443–467.
8. Yang, Z.; Gao, R.; Hu, N.; Chai, J.; Cheng, Y.; Zhang, L. The Prospective Two-Dimensional Graphene Nanosheets: Preparation, Functionalization, and Applications. *Nano-Micro Lett.* **2012**, *4*, 1–9.
9. Lee, D. Y.; Khatun, Z.; Lee, J.-H.; Lee, Y-k.; In, I. Blood Compatible Graphene/Heparin Conjugate through Noncovalent Chemistry. *Biomacromolecules* **2011**, *12*, 336–341.
10. Shao, Y.; Wang, J.; Wu, H.; Liu, J.; Aksay, I. A.; Lin, Y. Graphene Based Electrochemical Sensors and Biosensors: A Review. *Electroanalysis* **2010**, *22*, 1027–1036.
11. Bao, H.; Pan, Y.; Ping, Y.; Sahoo, N. G.; Wu, T.; Li, L. Chitosan-Functionalized Graphene Oxide as a Nanocarrierfor Drug and Gene Delivery. *Small* **2011**, *7*, 1569–1578.
12. Tang, Z.; Wu, H.; Cort, J. R.; Buchko, G. W.; Zhang, Y.; Shao, Y. Constraint of DNA on Functionalized Graphene Improves Its Biostability and Specificity. *Small* **2010**, *11*, 1205–1209.
13. Kong, W. H.; Sung, D. K.; Kim, K. S.; Jung, H. S.; Gho, E. J.; Yun, S. H. Self-Assembled Complex of Probe Peptide—*E. Coli* RNA I Conjugate and Nano Graphene Oxide for Apoptosis Diagnosis. *Biomaterials* **2012**, *33*, 7556–7564.

14. Kelkar, S. S.; Reineke, T. M. Theranostics: Combining Imaging and Therapy. *Bioconjugate Chem.* **2011**, *22*, 1879–1903.
15. Chen, M.-L.; He, Y.-J.; Chen, X.-W.; Wang, J.-H. Quantum-Dot-Conjugated Graphene as a Probe for Simultaneous Cancer-Targeted Fluorescent Imaging, Tracking, and Monitoring Drug Delivery. *Bioconjugate Chem.* **2013**, *24*, 387–397.
16. Nurunnabi, M.; Khatun, Z.; Reeck, G. R.; Lee, D. Y.; Lee, Y-k. Near Infra-Red Photoluminescent Graphene Nanoparticle Greatly Expands Use in Noninvasive Biomedical Imaging. *Chem. Commun.* **2013**, *49*, 5079–5081.
17. Liu, J. H.; Yang, S. T.; Wang, H.; Chang, Y.; Cao, A.; Liu, Y. Effect of Size and Dose on the Biodistribution of Graphene Oxide in Mice. *Nanomedicine* **2012**, *7*, 1801–1812.
18. Duch, M. C.; Budinger, G. R. S.; Liang, Y. T.; Soberanes, S.; Urich, D.; Chiarella, S. E.; Campochiaro, L. A.; Gonzalez, A.; Chandel, N. S.; Hersam, M. C.; et al. Minimizing Oxidation and Stable Nanoscale Dispersion Improves the Biocompatibility of Graphene in the Lung. *Nano Lett.* **2011**, *11*, 5201–5207.
19. Jastrzębska, A. M.; Kurtycz, P.; Olszyna, A. R. Recent Advances in Graphene Family Materials Toxicity Investigations. *J. Nanopart. Res.* **2012**, *14*, 1320–1340.
20. Kakran, M.; Sahoo, N. G.; Bao, H.; Pan, Y.; Li, L. Functionalized Graphene Oxide as Nanocarrier for Loading and Delivery of Ellagic Acid. *Curr. Med. Chem.* **2011**, *18*, 4503–4512.
21. Yang, K.; Gong, H.; Shi, X.; Wan, J.; Zhang, Y.; Liu, Z. *In Vivo* Biodistributionand Toxicology of Functionalized Nanographene Oxide in Mice after Oral and Intraperitoneal Administration. *Biomaterials* **2013**, *34*, 2787–2795.
22. Yang, K.; Wan, J.; Zhang, S.; Zhang, Y.; Lee, S.-T.; Liu, Z. *In Vivo* Pharmacokinetics, Long-Term Biodistribution, and Toxicology of PEGylated Graphene in Mice. *ACS Nano* **2011**, *5*, 512–522.
23. Christensen, I. B.; Sun, Y.-P.; Juzenas, P. Carbon Dots as Antioxidants and Prooxidants. *J. Biomed. Nanotechnol.* **2011**, *7*, 667–676.
24. Chen, M. L.; Liu, J. W.; Hu, B.; Chen, M. L.; Wang, J. H. Conjugation of Quantum Dots with Graphene for Fluorescence Imaging of Live Cells. *Analyst* . **2011**, *136*, 4277–4283.
25. Wenjing, X.; Wenjing, F.; Hong, M.; Mo, Z.; Louzhen, F. Preparation of Fluorescent Graphene Quantum Dots as Biological Imaging Marker for Cells. *Acta Chim. Sin.* **2012**, *70*, 2169–2172.
26. Shen, H.; Zhang, L.; Liu, M.; Zhang, Z. Biomedical Applications of Graphene. *Theranostics* **2012**, *2*, 283–294.
27. Zhang, Z.; Zhang, J.; Chen, N.; Qu, L. Graphene Quantum Dots: An Emerging Material for Energy-Related Applications and Beyond. *Energy Environ. Sci.* **2012**, *5*, 8869–8890.
28. Lightcap, I. V.; Kamat, K. V. Fortification of CdSe Quantum Dots with Graphene Oxide Excited State Interactions and Light Energy Conversion. *J. Am. Chem. Soc.* **2012**, *134*, 7109–7116.
29. Dong, Y.; Li, G.; Zhou, N.; Wang, R.; Chi, Y.; Chen, G. Graphene Quantum Dot as a Green and Facile Sensor for Free Chlorine in Drinking Water. *Anal. Chem.* **2012**, *84*, 8378–8382.
30. Brozek, E. M.; Zharov, I. Internal Functionalization and Surface Modification of Vinylsilsesquioxane Nanoparticles. *Chem. Mater.* **2009**, *21*, 1451–1456.
31. Tang, L.; Ji, R.; Cao, X.; Lin, J.; Jiang, H.; Li, X.; Teng, K. S.; Luk, C. M.; Zeng, S.; Hao, J.; *et al*. Deep Ultraviolet Photoluminescence of Water-Soluble Self-Passivated Graphene Quantum Dots. *ACS Nano* **2012**, *6*, 5102–5110.
32. Cheng, H.; Zhao, Y.; Fan, Y.; Xie, X.; Qu, L.; Shi, G. Graphene-Quantum-Dot Assembled Nanotubes: A New Platform for Efficient Raman Enhancement. *ACS Nano* **2012**, *6*, 2237–2244.
33. Markovic, Z. M.; Ristic, B. Z.; Arsikin, K. M.; Klisic, D. J.; Harhaji-Trajkovic, L. M.; Odorovic-Markovic, B. M.; Kepic, D. P.; Kravic-Stevovic, T. K.; Jovanovic, S. P.; Milenkovic, M. M.; *et al*. Graphene Quantum Dots as Autophagy-Inducing Photodynamic Agents. *Biomaterials* **2012**, *33*, 7084–7092.
34. Shen, J.; Zhu, Y.; Yang, X.; Li, C. Graphene Quantum Dots: Emergent Nanolights for Bioimaging, Sensors, Catalysis and Photovoltaic Devices. *Chem. Commun.* **2012**, *48*, 3686–3699.
35. Trauzettel, B.; Bulaev, D. V.; Loss, D.; Burkard, G. Spin Qubits in Graphene Quantum Dots. *Nat. Phys.* **2007**, *3*, 192–196.
36. Shen, J.; Zhu, Y.; Yang, X.; Zong, J.; Zhang, J.; Li, C. One-pot Hydrothermal Synthesis of Graphene Quantum Dots Surface-Passivated by Polyethylene Glycol and Their Photoelectric Conversion under Near-Infrared Light. *New J. Chem.* **2012**, *36*, 97–101.
37. Li, Y.; Zhao, Y.; Cheng, H.; Hu, Y.; Shi, G.; Dai, L.; Qu, L. Nitrogen-Doped Graphene Quantum Dots with Oxygen-Rich Functional Groups. *J. Am. Chem. Soc.* **2012**, *134*, 15–18.
38. Liu, T.; Yacoub, R.; Taliaferro-Smith, L. D.; Sun, S.-Y.; Graham, T. R.; Dolan, R.; Lobo, C.; Tighiouart, M.; Yang, L.; Adams, A. Combinatorial Effects of Lapatinib and Rapamycin in Triple-Negative Breast Cancer Cells. *Mol. Cancer Ther.* **2011**, *10*, 1460–1469.
39. Liao, K. H.; Lin, Y. S.; Macosko, C. W.; Haynes, C. L. Cytotoxicity of Graphene Oxide and Graphene in Human Erythrocytes and Skin Fibroblasts. *Appl. Mater. Interfaces* **2011**, *3*, 2607–2615.
40. Chang, Y.; Yang, S.-T.; Liu, J.-H.; Dong, E.; Wang, Y.; Cao, A.; Liu, Y.; Wang, H. *In Vitro* Toxicity Evaluation of Graphene Oxide on A549 Cells. *Toxicol. Lett.* **2011**, *200*, 201–210.
41. Song, C. K.; Balakrishnan, P.; Shim, C-k.; Chung, S.-J.; Kim, D.-D. Enhanced *in Vitro* Cellular Uptake of P-gp Substrate by Poloxamer-Modified Liposomes (PMLs) in MDR Cancer Cells. *J. Microencapsulation* **2011**, *28*, 575–581.
42. Nurunnabi, M.; Cho, K. J.; Choi, J. S.; Huh, K. M.; Lee, Y. Targeted Near-IR QDs-loaded Micelles for Cancer Therapy and Imaging. *Biomaterials* **2010**, *31*, 5436–5444.
43. Kim, J. S.; Cho, K. J.; Tran, T. H.; Nurunnabi, M.; Moon, T. H.; Hong, S. M. *In Vivo* NIR Imaging with CdTe/CdSe Quantum Dots Entrapped in PLGA Nanospheres. *J. Colloid Interface Sci.* **2011**, *353*, 363–371.
44. Michelle, L.; Peter, L. C.; Hisataka, K. Clearance Properties of Nano-sized Particles and Molecules as Imaging Agents: Considerations and Caveats. *Nanomedicine (London)* **2008**, *3*, 703–717.
45. Palevsky, P. M. Dialysis Modality and Dosing Strategy in Acute Renal Failure. *Semin. Dial.* **2006**, *19*, 165–170.
46. Peng, J.; Gao, W.; Gupta, B. K.; Liu, Z.; Romero-Aburto, R.; Ge, L.; Song, L.; Alemany, L. B.; Zhan, X.; Gao, G.; et al. Graphene Quantum Dots Derived from Carbon Fibers. *Nano Lett.* **2012**, *12*, 844–849.
47. Kim, J.; Nurunnabi, M.; Oh, Y. J.; Park, S. Y.; Lee, Y. Herceptin Conjugated PCL-PEG-PCL Triblock Copolymer for Cancer Targeting and Imaging. *Macromol. Res.* **2012**, *20*, 875–882.
48. Khatun, Z.; Nurunnabi, M.; Cho, K. J; Lee, Y-k. Oral Delivery of Near-Infrared Quantum Dot Loaded Micelles for Non-invasive Biomedical Imaging. *ACS Appl. Mater. Interfaces* **2012**, *4*, 3880–3887.
49. Khatn, Z.; Nurunnabi, M.; Reeck, G. R.; Cho, K. J.; Lee, Y-k. Oral Delivery of Taurocholic Acid Linked Heparin-Docetaxel Conjugated for Cancer Therapy. *J. Controlled Release* **2013**, *170*, 74–82.